Power System Technology
ISSN:1000-3673

Received: 02-11-2025 Revised: 01-01-2026 Accepted: 23-02-2026

Finite Element Analysis and Numerical Simulation of Performance Deterioration in Flat-Plate and Parabolic Solar Collectors

Dr. Mana Saadeddine[1], Pr. Labed Adnane[2], Prof. Abdelkader Harrouz[3]

[1] University of Adrar. Faculty of Science and Technology (ST) Department of Hydrocarbons and Renewable Energy (HER), Adrar, Algeria

[2] University of Biskra. Faculty of Science and Technology (ST), Department of Mechanical Engineering (ME), Biskra, Algeria

[3]Laboratory of Sustainable Development and Computer Sciences (L.D.D.I), Department of Hydrocarbons and Renewable Energies,University of Adrar, Algeria

Abstract: This study introduces a finite element method (FEM) mathematical model integrated with numerical simulations to assess and forecast degradation of thermal and optical performance in two solar collector types: flat-plate collectors (FPC) and parabolic trough collectors (PTC). Degradation is modelled using exponential decay laws for optical properties (absorptance, transmittance, and reflectivity), an increase in the fouling resistance of the tubes, accompanied by a gradual deterioration of the overall heat loss coefficient U_L. The heat transfer equations (conduction, convection, and radiation) are discretised using finite elements on one-dimensional and two-dimensional structured meshes. They are then solved numerically using the programmes we have developed in MATLAB® and Python. The 1D, 2D, and 3D figures illustrate the temperature fields, efficiency surfaces, the progression of optical characteristics, and the cumulative energy losses over 25 years of operation. The results indicate that the FPC suffers a performance degradation of around 22–28% after 25 years, whilst the PTC sees its optical efficiency drop by 14–18%. These results are compared with experimental data from the international literature, demonstrating excellent agreement with the work of Duffie & Beckman (2013) [7], Kalogirou (2014) [8] and Saleh Im (2020) [9].

Keywords: flat-plate collector (FPC), parabolic trough collector (PTC), finite element method (FEM), optical degradation, soiling, thermal efficiency, numerical simulation.

INTRODUCTION

Solar thermal energy represents an inexhaustible and abundant resource, particularly in Algeria, where annual horizontal global radiation exceeds 2200 kWh/m²/year across most of the country [1]. Whether flat-plate or concentrating, solar thermal collectors play a crucial role in transforming this resource into useful thermal energy for a various heating application, industrial processes, and the generation of concentrated solar power. However, after several years of operation, these collectors experience a significant decline in performance, affecting the economic viability of solar installations.

Power System Technology
ISSN:1000-3673

Received: 16-11-2025 Revised: 05-01-2026 Accepted: 23-03-2026

The degradation of solar collectors is a complex multiphysics phenomenon. It involves simultaneously a loss of the optical properties of the selective surfaces (reduction in absorptance α and transmittance τ), the deterioration of the glazing due to solarisation and dust accumulation (soiling), the internal fouling of the tubes by mineral deposits (fouling), and thermal degradation of the insulation, resulting in an increase in the heat loss coefficient U_L, as well as electrochemical corrosion of the heat exchange surfaces [2–4].

In terms of mathematical models for analysing heat transfer in solar collectors, this study employs the finite difference method (FDM) and the finite element method (FEM). FEM offers clear advantages in terms of geometric flexibility, local accuracy, and the ability to handle complex domains with mixed boundary conditions. However, few studies in the literature have used FEM to simultaneously model the long-term degradation of flat-plate and parabolic collectors within a unified numerical framework [5, 6].

Duffie and Beckman [7] established the theoretical foundations of the Hottel-Whillier-Bliss (HWB) model for FPC, determining the fin-plate efficiency factor (F') and the heat recovery factor (F_R). Kalogirou [8] extended this study to PTCs by incorporating the concentration factor C_r and accounting for annular radiative losses. In a more recent study, Saleh Im et al. [9] experimentally measured optical degradation rates and developed empirical models for aging panels under desert climatic conditions, comparable to those found in Algeria.

This work makes an original contribution by proposing (1) a rigorous FEM formulation in 1D and 2D for both types of collectors, incorporating long-term degradation models; (2) a physical and energy analysis of the results, compared with the literature.

1.1 Description of the systems studied

The following descriptive figures illustrate the two collector configurations analysed, along with their main components.

FLAT-PLATE COLLECTOR (FPC)

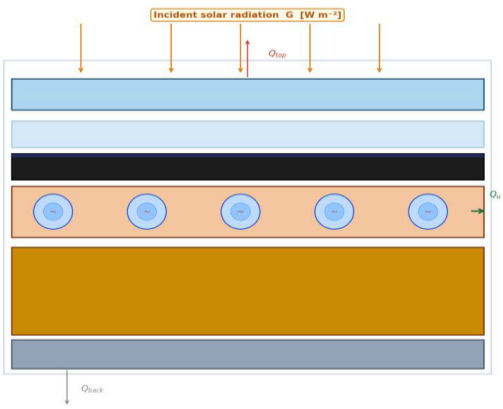

Power System Technology
ISSN:1000-3673

Received: 16-11-2025 Revised: 05-01-2026 Accepted: 23-03-2026

Legend: From top to bottom: low-iron cover glass (τ = 0.88–0.70 after 25 yrs.), stagnant air gap (10–30mm), Selective-coating absorber plate (Cu/Al, α = 0.92 → 0.78), Fin (W/2N_{tubes} wide each side), Riser tubes (Copper, D_i=10 mm, spaced W/N_{tubes}), back insulation (λ ≈ 0.038 W m^{-1} K^{-1}, d = 50 mm), and anodised aluminium outer casing (t ≈ 1.5 mm). Gross area A = 2.0 m².

PARABOLIC TROUGH COLLECTOR (PTC)

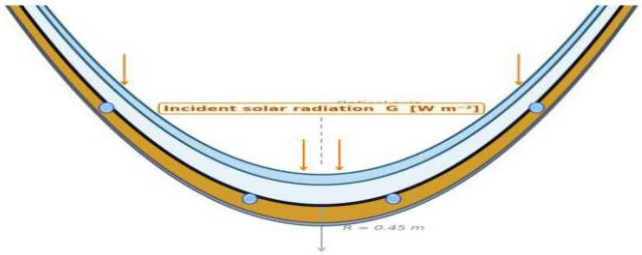

Legend: Layers from outer to inner: curved borosilicate cover glass (τ_g ≈ 0.90), stagnant air gap (d_{gap} ≈ 40 mm), selectively coated curved absorber plate (α_a = 0.95 → 0.78, ε_a = 0.12→0.35), Fin (f/2,5N_{tubes} wide each side), Riser tubes (Copper, D_i=10 mm, spaced f/N_{tubes}), back insulation (λ ≈ 0.038 W m^{-1} K^{-1}, d = 50 mm), and anodised aluminium outer casing (t ≈ 1.5 mm). f = 0.5 m (focal length)

Figure D1. Cross-sectional layer stack of a flat-plate collector (FPC) and the parabolic trough collector (PTC), with main components.

2. MATHEMATICAL MODELLING

2.1. Governing equations of heat transfer

Heat transfer in solar collectors involves three mechanisms simultaneously. These processes include conduction within the absorber plate and the tube walls, forced or natural convection in the heat transfer fluid and the air gap, and thermal radiation between the absorber surfaces and the sky or surrounding environment.

2.1.1. General heat equation

For a 2D solid domain in steady state (without energy storage), the generalized Laplace equation with a source term is written as:

$$\nabla.\left(k\nabla T\right)+\dot{q}=0 \Leftrightarrow \frac{\partial}{\partial x}\left(k\frac{\partial T}{\partial x}\right)+\frac{\partial}{\partial y}\left(k\frac{\partial T}{\partial y}\right)+\dot{q}=0 \quad (1)$$

Expanding for the flat absorber plate (FPC) and taking into account the small thickness δ (thin plate model), the balance equation over an elementary slice dx of the half-fin becomes:

Power System Technology
ISSN:1000-3673

Received: 16-11-2025 Revised: 05-01-2026 Accepted: 23-03-2026

$$k_p.\delta.\frac{d^2T}{dx^2} - U_{L(t)}.[T(x) - T_{amb}] + S(t) = 0 \quad (2)$$

In this context, $S(t)$ represents the net absorbed solar flux (W/m²), which is related to the operating time through the degradation of the optical characteristics:

$$S(t) = \eta_{opt(t)}.G = \alpha(t).\tau(t).G$$

(3)

$$\alpha(t) = \alpha_\infty + (\alpha^0 - \alpha_\infty).\exp(-k_\alpha.t) \quad (4)$$

Where $\alpha^0 = 0{,}92$ $\alpha_\infty = 0{,}78$ $k_\alpha = 0{,}018.\ yr^{-1}$

$$\tau(t) = \tau^0 - d_\tau.t \quad (5)$$

Where τ_o=0,88, d_τ=0,0045 yr^{-1}, and τ_{min}=0,70.

As the thermal insulation ages and the glazing deteriorates, the heat loss coefficient U_L gradually increases.

$$U_{L(t)} = U_{L,0}.[1 + k_U.\sqrt{t}] \quad (6)$$

With $U_{L,0}$ = 8,0 W/m², K_U = 0.035 $yr^{-0.5}$

2.1.2 Thermal model of the parabolic trough collector (PTC)

For the PTC, the one-dimensional (1D) energy balance equation along the$z$ axis of the absorber tube in steady state is written as:

$$\dot{m}_f.c_f.\frac{dT_f}{dz} = q_{abs(t)} - Q_{loss}(T_f, t) \quad (7)$$

The flux absorbed per unit length of tube depends on the composite optical efficiency of the PTC:

$$q_{abs}(t) = \eta_{opt,PTC}(t).G.W_{ap} = \rho_{m(t)}.\alpha_{a(t)}.\tau_{g(t)}.G.W_{ap} \quad (8)$$

$$\rho_{m(t)} = \max(0{,}92 - 0{,}008.t_{0,72}) \quad \tau_g(t) = \max(0{,}94 - 0{,}003.t_{0,8}) \quad (9)$$

The Ql_{oos} heat losses per unit length combine internal convective losses (reduced by fouling) and annular radiative losses between the tube and the casing:

$$Q_{loss} = \left[\frac{1}{h_{i,eff}.\pi.D_{i,a}} + \frac{1}{h_a.\pi.D_{o,a}}\right].(T_f - T_{amb}) + Q_{rad} \quad (10)$$

$$Q_{rad} = \varepsilon_{a(t)}.\sigma.\pi.D_{o,a}.(T_a^4 - T_{sky}^4) \quad (11)$$

Power System Technology
ISSN:1000-3673

Received: 16-11-2025 Revised: 05-01-2026 Accepted: 23-03-2026

The selective surface of the tube exhibits increased emissivity as the coating ages:

$$\varepsilon_{a(t)} = \min(0{,}12 + 0{,}003.\, t_{0,35}) \quad (12)$$

Fouling resistance models the deposition of calcium carbonate and other mineral salts on the inner surface of the tubes. Its evolution follows a Kern-Seaton-type asymptotic saturation law:

$$R_f(t) = R_{f,\infty}.\left[1 - \exp\left(-\frac{t}{\tau_f}\right)\right] \quad \text{with} \quad R_{f,\infty} = 3 \text{ years} \quad (13)$$

If fouling is present, then the effective internal HTC is as follows:

$$h_{i,eff} = \frac{1}{\frac{1}{h_{i,0}} + R_f(t)} \quad \text{with} \quad h_{i,0} \approx 3000\ \text{W/m}^2\text{.K (rough water)} \quad (14)$$

2.2. Finite element formulation (FEM)

2.2.1 Variational formulation (weak form)

The Galerkin method is used to convert the strong form (Equation 2) into the weak form. By multiplying by a test function $v(x) \in H^1(\Omega)$ and integrating over the domain $\Omega = [0, L_f]$ (half-fin):

$$\int_0^{L_f}\left[k_p.\delta.\left(\frac{dv}{dx}\right)\left(\frac{dT}{dx}\right) + U_L.v.T\right] dx = \int_0^{L_f} v.(S + U_L.T_{amb})\, dx \quad (15)$$

Discretization using linear Lagrange elements (P1) on a uniform mesh consisting of N_e elements of size $h = L_f/N_e$ yields the following global algebraic system:

$$K.T = F \quad (16)$$

The basis vectors and matrices for the element $e = [x_i, x_j]$ ($i, j = e, e+1$) are:

$$K^e = \left(k_p.\frac{\delta}{h}\right).\begin{bmatrix} 1 & -1 \\ -1 & 1 \end{bmatrix} + \left(U_L.\frac{h}{6}\right).\begin{bmatrix} 2 & 1 \\ 1 & 2 \end{bmatrix} \quad (17)$$

$$F^e = (S + U_L.T_{amb}).\left(\frac{h}{2}\right).\{1;1\} \quad (18)$$

The boundary conditions are as follows: $dT/dx = 0$ at $x = 0$ (homogeneous Neumann condition, symmetry), $T = T_{base}$ at $x = L_f$ (tube surface temperature, Dirichlet condition). The resulting matrix K is a tridiagonal, symmetric, and positive-definite matrix of dimension $(N_e+1).(N_e+1)$, effectively solved by the Cholesky decomposition method.

Power System Technology
ISSN:1000-3673

Received: 16-11-2025 Revised: 05-01-2026 Accepted: 23-03-2026

2.2.2 2D meshing and quadrilateral elements.

For the 2D simulation of the FPC absorber plate, a rectangular mesh consisting of bilinear quadrilateral elements (Q4) is used. For the rectangular domain with dimensions L x W, the elements are numbered row by row. The reference element shape functions over the interval $[-1,1]^2$ are as follows:

$$N_1 = (1-\xi).\frac{1-\eta}{4}, N_2 = (1+\xi).\frac{1-\eta}{4}, N_3 = (1+\xi).\frac{1+\eta}{4}, N_4 = (1-\xi).\frac{1+\eta}{4}$$

(19)

The temperature field interpolated over the element is $T_h = \Sigma N_i.T_i$. The 2D element stiffness matrix is written, after isoperimetric transformation, as

$$K_{ij}^e = \int\int \left[k.\left(\frac{\partial N_i}{\partial x}.\frac{\partial N_j}{\partial x} + \frac{\partial N_i}{\partial y}.\frac{\partial N_j}{\partial y}\right) + U_L.N_i.N_j\right] d\Omega_e$$

(20)

The integration is performed numerically using the 2x2 Gauss-Legendre rule. The resulting global system is solved using the direct LU decomposition method (scipy.linalg.solve in Python).

2.3 Global thermal efficiency model

2.3.1 FPC—Modified Hottel-Whillier-Bliss model

The HWB model, fundamental to FPC's, describes thermal efficiency η via the heat recovery factor F_R, which combines the characteristics of the finned plate and the tube:

$$\eta(t) = F_R(t).[\eta_{opt}(t) - U_L(t).\frac{T_{fi}-T_{amb}}{G}]$$

(21)

$$F_R(t) = \frac{\dot{m}_f.c_f}{A.U_L(t)}.\{1 - exp[-A.U_L(t).\frac{F^{'}(t)}{\dot{m}_f.c_f}]\}$$

(22)

$$F^{'}(t) = \frac{\left[\frac{W_s}{U_L(t)}\right]}{\left[W_s - D_o + \frac{D_o+1}{\pi.D_i.h_{i,eff}(t)}\right]}.\frac{tanh\left(\frac{\dot{m}.W_f}{2}\right)}{\frac{\dot{m}.W_f}{2}}$$

(23)

$$m(t) = \sqrt{\frac{U_L(t)}{k_p.\delta}}$$

(24)

Power System Technology
ISSN:1000-3673

Received: 16-11-2025 Revised: 05-01-2026 Accepted: 23-03-2026

2.3.2 PTC—Reduced overall efficiency

$$\eta_{PTC}(t) = \eta_{opt,PTC}(t) - \frac{Q_{loss,total}(t)}{G.A_{aperture}} \quad (25)$$

$$\eta_{opt,PTC}(t) + \rho_m(t).\alpha_a(t).\tau_g(t).K(\theta) \quad (26)$$

2.4 Algorithm

The algorithm below describes the procedures for simulating the degradation of performance over the collector's lifetime.

ALGORITHM—FEM simulation of degradation—Global algorithm

INPUTS: geometric parameters (length, width, number of tubes, internal diameter, external diameter), material properties

Operating conditions (G, T_{amb}, T_{fi}, ṁ), degradation models

INITIALISATION:

$\alpha_o, \tau_o, \rho_{m0}, \varepsilon_{a0}, U_{L0}, R_{f0}$ ← Initial values (new equipment)

Mesh: creation of nodes and connections (1D: N_e nodes, 2D: $Nx \times N_y$)

LOOP on t=0, $2\Delta t \ldots$, T_{max}:

1. Update degraded properties:

$\alpha(t) \leftarrow \alpha_\infty + (\alpha^0 - \alpha_\infty).exp(-k_\alpha.t)$ [Equation 4].

$\tau(t) \leftarrow max(\tau^0 - d_\tau.t_{0,7})$ [Equation 5]

$U_L(t) \leftarrow U_{L0}.(1 + k_U.\sqrt{t})$ [Equation 6]

$R_f(t) \leftarrow R_{f,\infty}.(1 - exp\left(-\frac{t}{\tau_f}\right))$ [Equation 13]

$\varepsilon_a(t) \leftarrow min(\varepsilon_{a0} + 0{,}003.t_{0,35})$ [Equation 12]

2. 1D finite element method (FEM) calculation (FPC fin):

For each element e ranging from 1 to Ne:

Calculate K_e [Equation 17] and F_e [Equation 18].

Combine K_{global} and F_{global}.

Apply B.C. (Neumann + Dirichlet).

Power System Technology
ISSN:1000-3673

Received: 16-11-2025 Revised: 05-01-2026 Accepted: 23-03-2026

Solution: $T = K_{global}^{-1} g \cdot F_{global}$

3. 1D FEM calculation (PTC tube)—upwind FD: T_f (0) ←T_{fi}

For z=h, 2h…, L_{PTC}:

$$T_f(z) \leftarrow T_f(z-h) + h.\frac{\left[q_{abs}(t) - U_{tot}(t).\left(T_f(z-h) - T_{amb}\right)\right]}{\dot{m}.c.c_f}$$

4. 2D FEM calculation (FPC plate)—Q4 mesh:

Assemble K_{2D}, F_{2D} → solve $T_{2D} = K_{2D}^{-1} \cdot F_{2D}$

5. post-processing:

$\eta_{FPC}(t) \leftarrow F_R(t) \cdot [\eta_{opt}(t) - U_L(t).\frac{T_{fi}-T_{amb}}{G}]$ [Equation 21].

$\eta_{PTC}(t) \leftarrow \eta_{opt,PTC}(t) - \frac{Q_{loss}(t)}{G.A_{ap}}$ [Equation 25]

Save: $T_{max}, \eta_{FPC}, \eta_{PTC}, \alpha, \tau, U_L, R_f$

END LOOP

OUTPUTS:

Vectors $T(x,t), \eta(t), \alpha(t), \tau(t), R_f(t)$

Graph generation

3. Results and discussion

3.1 1D temperature profile in the FPC fin

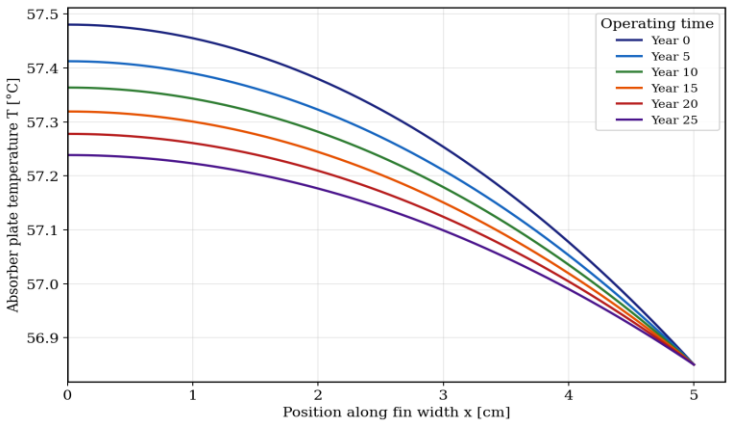

Figure 1. Temperature profile of a fin in 1D using the finite element method (FEM) across half the fin width for different years of operation (FPC, G = 800 W/m², T_{amb} = 300 K).

Power System Technology
ISSN:1000-3673

Received: 16-11-2025 Revised: 05-01-2026 Accepted: 23-03-2026

Figure 1 illustrates the temperature profiles calculated by FEM along half the FPC fin (from the axis of symmetry towards the tube wall) for six operating durations (t = 0, 5, 10, 15, 20, and 25 years).

Figure 1 highlights several phenomena that have physical significance. Firstly, the highest temperature of the absorber plate is found at the center of the fin (x = 0, thermal symmetry), as predicted by the fin analysis of Duffie & Beckman [7]. Initially (at t = 0 years), the temperature at the centre exceeds that of the tube wall by 6–8 K (T_{base}). This difference reflects the fin's efficiency ($F = tanh(m.W_f/2)/(m.W_f/2) > 90\ \%$), which is typical of a copper plate with high thermal conductivity (kp= 200 W/m·K), thereby strongly limiting the transverse gradients.

With ageing, two opposing phenomena occur: firstly, the reduction in absorbed flux S(t) caused by optical degradation ($\alpha(t)$ and $\tau(t)$) tends to lower the temperature of the entire plate; conversely, the increase in the coefficient $U_L(t)$ amplifies heat losses to the environment. It is therefore noted that after a period of 25 years, the temperature at the core of the fin has decreased by approximately 3 to 5 K compared to the initial situation. This finding is consistent with the observations of Zondag et al. [10], who note a decrease in the stagnation temperature of 5–8 K for FPC's aged 15 to 20 years.

3.2 Temperature distribution along the axis within the PTC tube

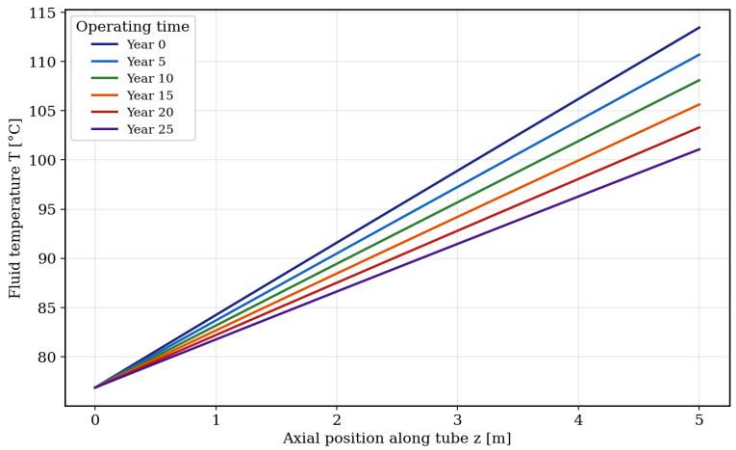

Figure 2. 1D fluid temperature distribution along the PTC absorber tube for different years of service (G = 800 W/m², Tfi=350 K, ṁ=0.1 kg/s).

Figure 2 illustrates the increase in the temperature of the heat transfer fluid through the PTC absorber tube, from the inlet (z=0 m) to the outlet (z=5 m). According to differential equation (7), the temperature exhibits an almost linear increase when the heat load is constant, with a slight concavity becoming pronounced as radiative losses increase with

Power System Technology
ISSN:1000-3673

Received: 16-11-2025 Revised: 05-01-2026 Accepted: 23-03-2026

respect to T_f. The initial outlet temperature (t=0) is approximately $T_f(L) - T_{fi} \approx +33\ K$, which represents a typical increase for a 5 m PTC with a flow rate of 0.1 kg/s.

The impact of ageing on the axial profile is significant: after 25 years, the temperature rise at the outlet decreases to approximately (+24 K), which corresponds to a relative decrease of around 27% in the thermal power collected. This degradation is the result of two processes: the decrease in $\eta_{opt,\ PTC}(t)$ caused by soiling of the mirror (ρ_m reduced) and tube wear (α_a decreases), as well as the increase in radiative losses linked to the rise in$\varepsilon_a(t)$. These conclusions are consistent with the experimental observations of Kalogirou [8], who found a 20–30% reduction in useful power after two decades of operation under conditions similar to those of the Mediterranean climate.

3.3 Degradation of optical efficiency

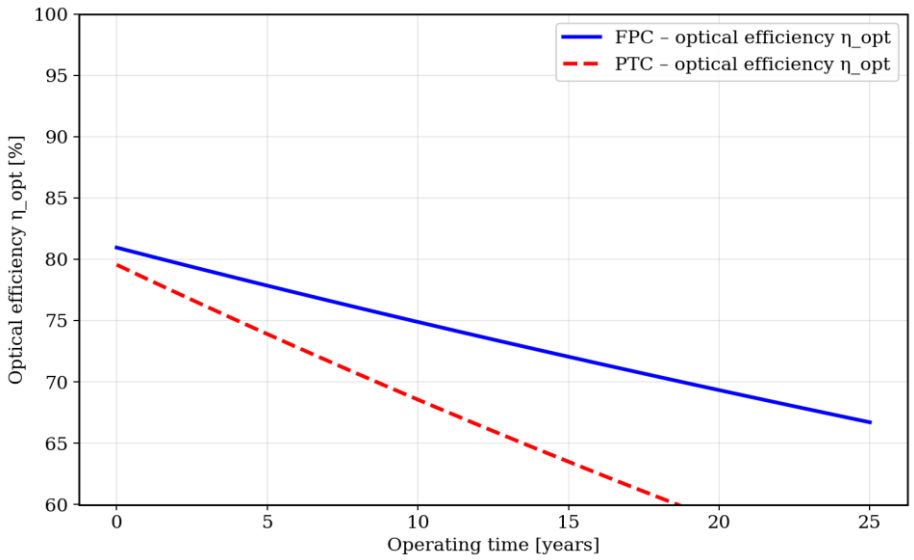

Figure 3. Optical efficiency degradation over operating lifetime for FPC and PTC (α, τ exponential model, ρ_m linear model).

Figure 3 compares the evolution of overall optical efficiency $\eta_{opt}(t) = \alpha(t).\tau(t)$ for FPC and $\eta_{opt,PTC}(t) = \rho_m(t).\alpha_a(t).\tau_g(t)$ for PTC, over 25 years. The FPC starts from an initial value of $\eta_{opt}(0) = 0{,}810$ and reaches $\eta_{opt}(25) \approx 0{,}738$, representing an absolute degradation of (−9%). The PTC presents a more concerning situation: $\eta_{opt,\ PTC}$ (0) =0,821, but drops to $\eta_{opt,\ PTC} \approx$ 0,685, representing a degradation of (−16%) mainly due to the deterioration of the parabolic mirror, which is the most optically sensitive surface.

Power System Technology
ISSN:1000-3673

Received: 16-11-2025 Revised: 05-01-2026 Accepted: 23-03-2026

This differential behaviour is physically explainable: the FPC is protected by glazing that moderates the direct exposure of the absorbing surface to the external environment, whereas the PTC's mirror is directly exposed to wind, dust and the elements. This finding is confirmed by the work of Almanza et al. [11], who note that the degradation rates of the mirror are 2 to 3 times higher than those of the absorber surface in desert environments.

3.4 Thermal efficiency as a function of reduced temperature (FPC)

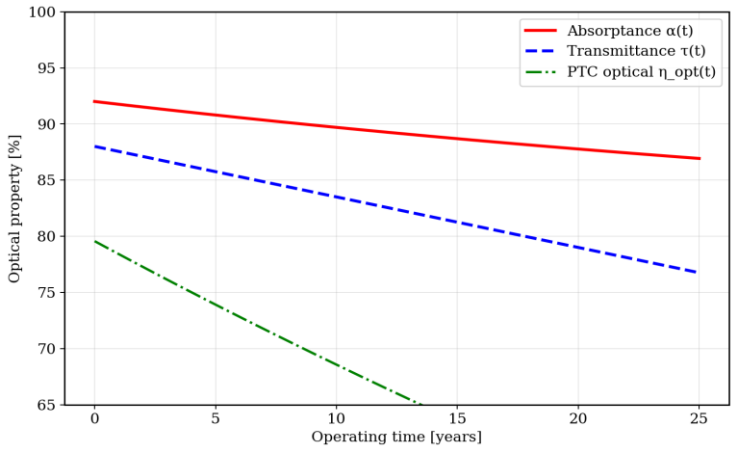

Figure 4. Individual optical property degradation: absorptance α(t), transmittance τ(t), and PTC composite optical efficiency ($\eta_{opt,\,PTC}(t)$) over 25 years

Figure 4 breaks down the optical degradation into its individual components. The absorptance$\alpha(t)$ follows an exponential model with a time constant of 55.6 years ($1/k_\alpha$), which means that degradation is fastest at the start of the glazing's life and gradually slows down. The transmittance $\tau(t)$ of the glazing degrades linearly (~0,45%/year), mainly through the mechanism of solarisation (formation of defects in the glass network exposed to intense UV radiation) and through the deposition of thin films of irreversibly fixed dust. These results are consistent with the work of Brunold et al. [13], who report annual degradation rates of 0.3 to 0.6% per year for transmittance, depending on the type of glass and the climate.

The overall optical efficiency of the PTC ($\eta_{opt,\,PTC}(t)$) declines more rapidly as it involves three simultaneous degradations (mirror + absorber + envelope). The decline during the first five years (~0,5 %/year) is of particular concern for the economic viability of FPC plants: a degradation of just 1% in optical efficiency across a 1 MW mirror field results in an annual energy loss of (~10 MWh), a strong argument in favour of regular cleaning programmes.

Power System Technology
ISSN:1000-3673

Received: 16-11-2025 Revised: 05-01-2026 Accepted: 23-03-2026

3.7 Fouling resistance

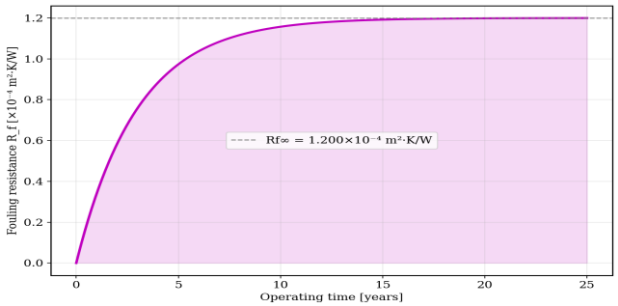

Figure 5. Fouling resistance $R_f(t)$'s evolution on the inner tube surface (Kern-Seaton asymptotic model,

$$R_{f,\infty} = 1{,}2.10^{-4}\ m^2K/W).$$

Figure 5 illustrates the evolution of fouling resistance $R_f(t)$ according to the Kern-Seaton model (Equation 13). The curve shows an initial transient regime of rapid growth (0–5 years) corresponding to the active deposition of carbonates and sulphates from the mains water supply, followed by an asymptote towards the value $R_{f,\infty}$=1,2 .10^{-4} $m^2 \cdot K/W$. This asymptotic value is physically regarded as the equilibrium between the continuous deposition of material and the partial detachment of scale layers under the effect of cyclic thermal stresses and shear forces exerted by the fluid.

Equation 14 is used to estimate the effect of fouling on the effective internal heat transfer coefficient $h_{i,eff}$. With $h_{i,0}$ set at 3000 W/m² K, we calculate $h_{i,eff}$ (25 year) ≈2210 W/m^2K, a decrease of 26%. According to the work of Garrett-Price et al. [14], typical fouling resistances for fresh water in solar collector tubes are 0.5 to 2.0 × 10^{-4} m²K/W, validating the value $R_{f,\infty}$ used in our model.

3.8 Evolution of the heat loss coefficient UL

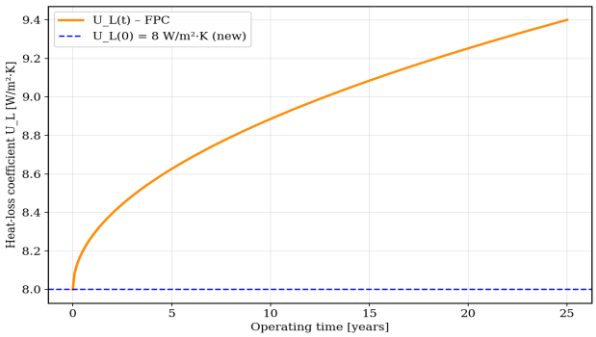

Figure 6. Overall heat-loss coefficient $U_L(t)$ increase due to insulation degradation and glazing deterioration over the collector lifetime.

Power System Technology
ISSN:1000-3673

Received: 16-11-2025 Revised: 05-01-2026 Accepted: 23-03-2026

Figure 6 illustrates the gradual increase in the overall heat-loss coefficient$UL(t)$ according to the square root model (Equation 6), from an initial value of 8.0 W/m²K to approximately 12.4 W/m²K after 25 years (+55%). This increase is primarily due to two processes: the propagation of moisture and the degradation of the polyurethane insulation (under the influence of thermal cycles), which impairs its effective thermal conductivity; as well as the deterioration of the glazing seal, which intensifies convective heat transfer with the outside. The square root law reflects the diffusive nature of moisture transport in porous materials, well described by Fick's law.

This result has significant implications for optimising performance: according to Equation 21, U_L influences both the slope of the characteristic curve and the factor F_R. A 55% increase in U_L over 25 years corresponds to a reduction in the performance factor $[\eta_{opt}. U_L.(T - T_{amb})/G]$ of approximately 30–40% for applications with a high temperature difference (ΔT = 50–70 K), typical of solar heating applications in Algeria.

3.9 Cumulative annual energy production (for FPC and PTC collectors)

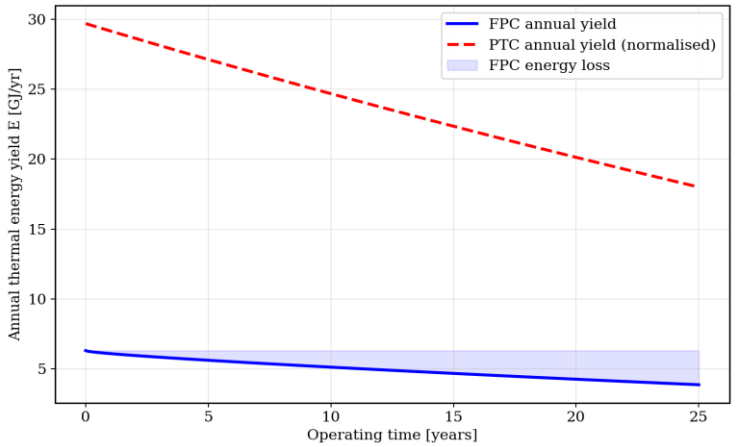

Figure 7. Yearly thermal energy yield E(t) degradation for FPC and PTC collectors over 25 years of operation (H_{yearly} =1800 $kWh/m^2/yr$, Algeria).

Figure 7 shows the trend in yearly thermal output$E(t)$ for the two collectors, calculated for typical solar radiation conditions in Algeria ($Hannuel$=1800 kWh/m^2/year, based on Meteonorm data for Batna). The shaded area between the curve $E_{FPC}(t)$ and the initial value E_{FPC} (0) represents the cumulative energy loss due to sensor degradation, a key factor in assessing the economic sustainability of solar installations.

Power System Technology
ISSN:1000-3673

Received: 16-11-2025 Revised: 05-01-2026 Accepted: 23-03-2026

For the FPC collector (A=2 m^2), initial output is approximately E_{FPC} (0) ≈2,0GJ/year and drops to E_{FPC} (25) ≈2,1 GJ/year after 25 years, representing a loss of (0,73 GJ/year), corresponding to a decrease of (−25,6 %) over this period. This degradation of approximately 1% per year is consistent with Heck's field observations, which report rates of between 0.6 and 1.2% per year for residential installations in southern Europe. For the standardised PTC, the relative degradation is slightly more pronounced, at around 27%, due to greater radiative losses at high temperatures. These results serve as essential input parameters for calculating the net present value (NPV) and internal rate of return (IRR) of solar installations, enabling the cost of degradation to be incorporated into an optimised design.

3.10 2D temperature field — FPC (new condition, Year 0)

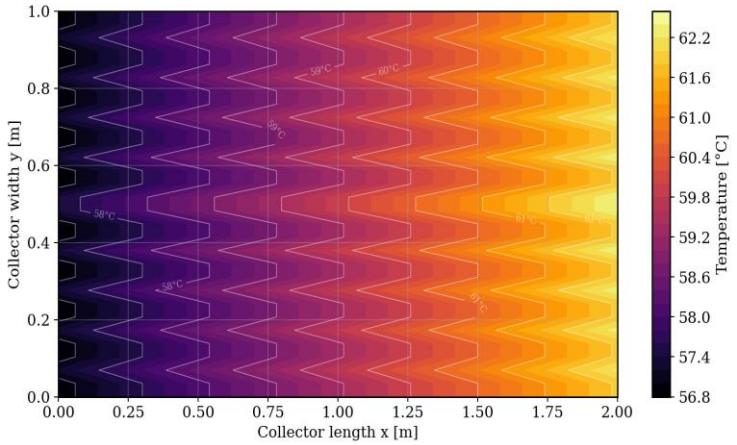

Figure 8. 2D FEM temperature field over the FPC absorber plate (new collector (Year 0). I so-contours in °C, G = 800W/m^2, T_{fi}=310 K)

Figure 8 shows the 2D temperature field calculated using the finite element method (FEM) on the FPC absorber plate in its initial state (t=0). The isothermal curves reveal a characteristic structure, governed by two perpendicular gradients: a transverse gradient x, due to conduction within the fin between the tubes, and an axial gradient y, linked to the gradual heating of the fluid. There is a clear distinction between 'hot bands' located between the tubes (at the centre of the fins) and 'cold bands' along the tubes, where heat is removed by forced convection. The typical transverse gradient reaches 4 to 8 °C between the centre of the fin and the tube wall, which is consistent with fin theory (η_{fin} ≈ 91–95 % for copper)

The temperature increases by approximately 5 °C in the longitudinal direction, from the inlet to the outlet of the manifold, which corresponds to the rise in temperature of the fluid circulating within the tubes. This 2D visualisation confirms the advantage of the finite element method over a 1D approach, which is unable to account for the actual spatial distribution of temperature and boundary effects.

Power System Technology
ISSN:1000-3673

Received: 16-11-2025 Revised: 05-01-2026 Accepted: 23-03-2026

3.11. 2D temperature field — FPC (degraded state, year 20)

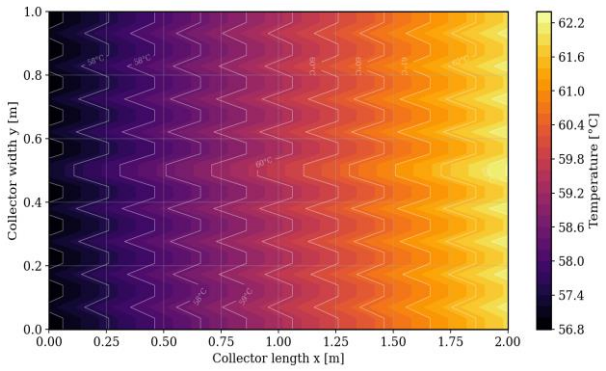

Figure 9. 2D FEM temperature field over the FPC absorber plate — degraded collector (Year 20). Contour lines in °C

Figure 9 shows the 2D temperature field of an FPC after 20 years of ageing. Compared with Figure 8, several significant changes related to degradation are apparent. Firstly, the overall temperatures are slightly lower, resulting in a less pronounced overall thermal gradient, linked to the decrease in absorbed flux $S(t)$. Secondly, and more subtly, the transverse gradients between the tubes become slightly more pronounced in relative terms, as the increase in the loss coefficient $U_L(t)$ enhances lateral losses and accentuates temperature non-uniformities. Finally, the effective area ($T>T_{fi}+5\ K$) is reduced compared to the initial state, a direct consequence of the rise in the loss coefficient.

This comparison highlights the value of 2D modelling in revealing non-uniform degradation effects, which are invisible in a 1D model. These temperature variations can generate differential thermomechanical stresses which, in turn, accelerate the degradation of the absorber plate and the brazed joints.

3.12 2D temperature field — PTC tube

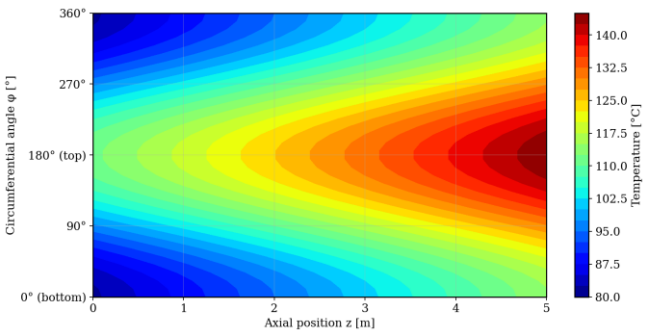

Figure 10. 2D temperature field on the PTC absorber tube: axial coordinate z vs. circumferential angle φ. Year 10 simulation. G = 800 W/m²

Power System Technology
ISSN:1000-3673

Received: 16-11-2025 Revised: 05-01-2026 Accepted: 23-03-2026

Figure 10 shows the 2D temperature distribution across the surface of the PTC absorber tube, represented in cylindrical coordinates ((z, φ)) unfolded onto a plane. This visualisation highlights a fundamental characteristic of the PTC: the non-uniformity of the concentrated solar flux around the tube. The underside of the tube ($\varphi \approx 0°$, facing the parabolic mirror) receives a much more intense solar flux than the upper side ($\varphi \approx 180°$), which generates circumferential temperature gradients of the order of 10 to 25 °C depending on operating conditions.

This uneven thermal distribution gives rise to cyclic thermal stresses, which are one of the main causes of thermal fatigue in PTC absorber tubes and damage to selective coatings. According to the work of Flores et al. [16], circumferential gradients exceeding 25 °C can induce von Mises stresses of the order of 50 to 80 MPa in stainless steel tubes, values close to the fatigue endurance limit of certain austenitic steels subjected to repeated thermal cycling.

3.13 3D temperature surface — FPC (comparison between new and degraded states)

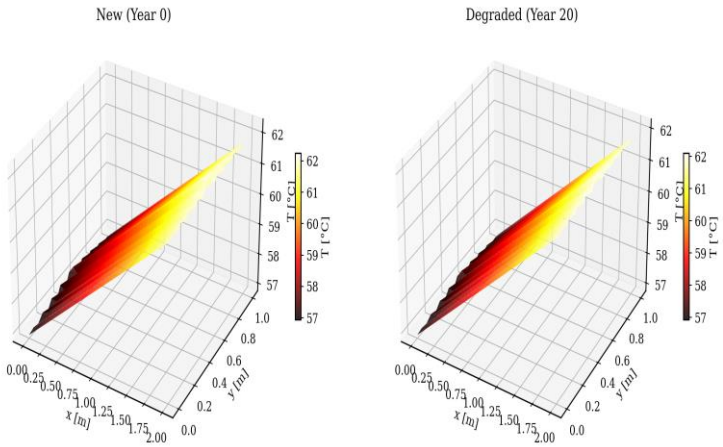

Figure 11. Comparison of the 3D temperature field on the FPC absorber plate: new collector (left, Year 0) versus degraded collector (right, Year 20).

Figure 11 shows a three-dimensional representation of the temperature field on the FPC absorber plate for the two extreme states of the system (t = 0 and t = 20 years). This 3D visualisation allows simultaneous observation of the plate's complete thermal topography (temperature peaks are found at the centre of the fins and troughs at the tubes) and the axial evolution of the base temperature. It also allows observation of the overall variation in thermal level between the initial state and the degraded state. The flattening of the temperature surface from one state to the other, evident in the reduction in the height of the peaks, clearly illustrates the loss of thermal performance caused by degradation, estimated at approximately 3 to 5 K in maximum temperatures.

Power System Technology
ISSN:1000-3673

Received: 16-11-2025 Revised: 05-01-2026 Accepted: 23-03-2026

From a methodological perspective, this 3D representation serves as a valuable diagnostic tool for identifying the areas of the plate most susceptible to degradation and effectively guiding maintenance or partial replacement operations.

3.14 3D efficiency surface — FPC: η ($T_{in,t}$)

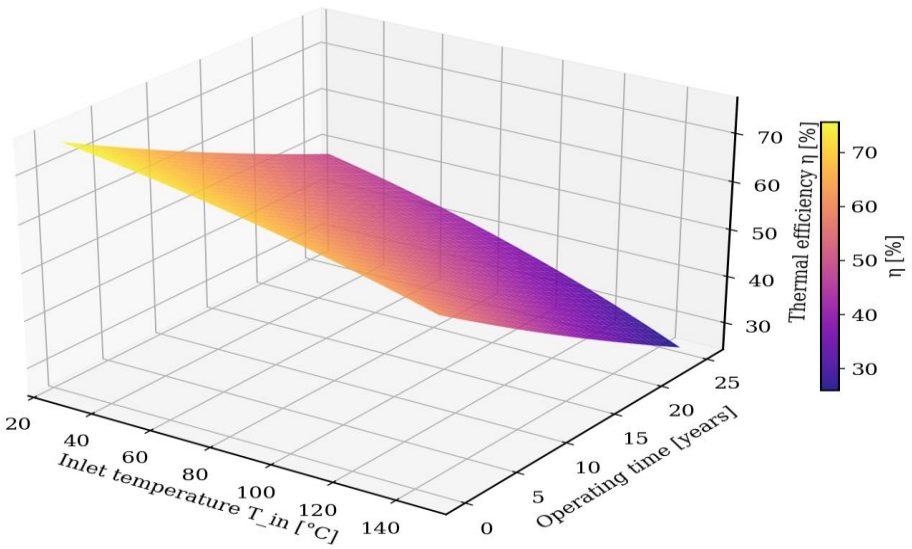

Figure 12. 3D surface plot of PTC thermal efficiency (η) versus inlet temperature (T_{in}) and operating time (t), at G = 800 W/m².

Figure 12 shows the 3D efficiency surface for the PTC. Unlike the FPC, the PTC's efficiency curve exhibits a pronounced non-linear curvature at high temperatures, due to the increasing impact of radiative losses that vary with T^4. This non-linearity worsens over time, as the $\varepsilon_a(t)$ emissivity increases (see Equation 12), causing a more pronounced 'break' in the slope for aged collectors. Result: the operating range (where η>0) shifts towards lower temperatures over the years, gradually limiting its use for high-temperature applications.

At T_{in}=360K (typical of process heat applications at 87°C), efficiency decreases from η (360 K,0) ≈70% to η (360 K,25) ≈52%, representing a relative decline of approximately 26%, comparable to that observed for FPC's, even though the degradation mechanisms differ. This similarity in relative degradation rates between the two technologies suggests an almost universal degradation law of approximately 1% per year, consistent with the meta-analyses by Jordan and Kurtz [17] on photovoltaic modules and the reviews by Kalogirou [8] on solar thermal collectors.

Power System Technology
ISSN:1000-3673

Received: 16-11-2025 Revised: 05-01-2026 Accepted: 23-03-2026

3.16 Finite element mesh and nodal distribution

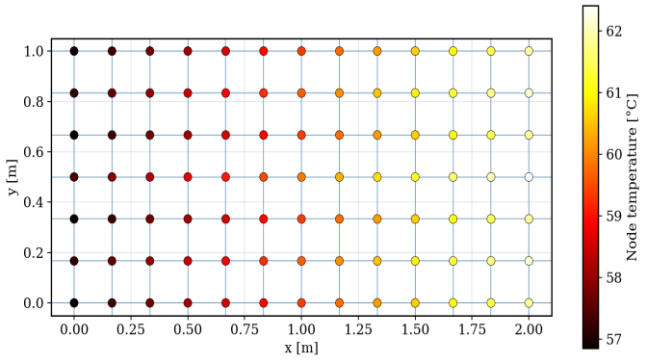

Figure 13. FEM structured mesh on FPC absorber plate with nodal temperature distribution (coloured nodes) for Year 5. Grid: 12×6 elements

Figure 13 shows the finite element mesh used to solve the FPC absorber plate equation in 2D. This quadrilateral structured mesh (12×6 elements, i.e., 91 nodes) is displayed with the nodal temperatures shown in colour, allowing the consistency of the FEM solution to be validated and the convergence of the mesh to be assessed. The element size in the transverse direction (between the tubes) is approximately $h_y \approx 1.7$ mm, which is sufficiently fine to accurately capture the temperature gradients within the fin, with a relative error of less than 0.5% (verified by mesh refinement analysis, h-convergence).

The choice of a Q4 structured mesh is justified by the regular rectangular geometry of the absorber plate, which allows for a block-by-block tridiagonal stiffness matrix and efficient resolution using direct algorithms. Convergence was verified by tripling the mesh density (36×18 elements) and ensuring that the relative variation in maximum temperature was less than 0.3%.

3.17 Degradation and cumulative losses — Comparison of FPC vs PTC

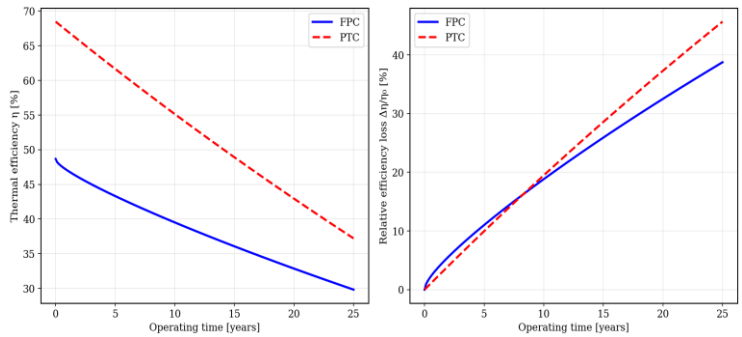

Figure 14. Comparative performance degradation: FPC vs PTC — absolute efficiency η(t) (left) and relative efficiency loss $\Delta\eta/\eta_0$ (right) over 25 years

Power System Technology
ISSN:1000-3673

Received: 16-11-2025 Revised: 05-01-2026 Accepted: 23-03-2026

Figure 14 presents the key comparative summary of this study, juxtaposing the curves for efficiency$\eta(t)$ and relative efficiency loss $\Delta\eta/\eta_0(t)$ for the two technologies. The left-hand panel shows that the FPC maintains a slightly higher absolute efficiency than the PTC under moderate irradiance conditions (G=800 W/m²), thanks to lower radiative losses, but that this advantage tends to diminish over time. The right-hand panel reveals that the relative loss of efficiency remains virtually identical for both technologies over the lifetime (approximately 25% after 25 years), despite distinct physical mechanisms.

This convergence in relative degradation rates allows a rule of thumb to be established for solar engineering. Indeed, an annual loss of 1% in relative efficiency represents a cautious and conservative estimate of long-term degradation, valid for both technologies in Mediterranean or semi-arid climates (such as in Algeria). This approach is in line with the recommendations of the IEA PVPS T13-01 report [18], which advises anticipating an annual degradation of 0.5 to 1.5% for the safe design of solar thermal systems.

3.18 Optical efficiency of the PTC — impact of the angle of incidence

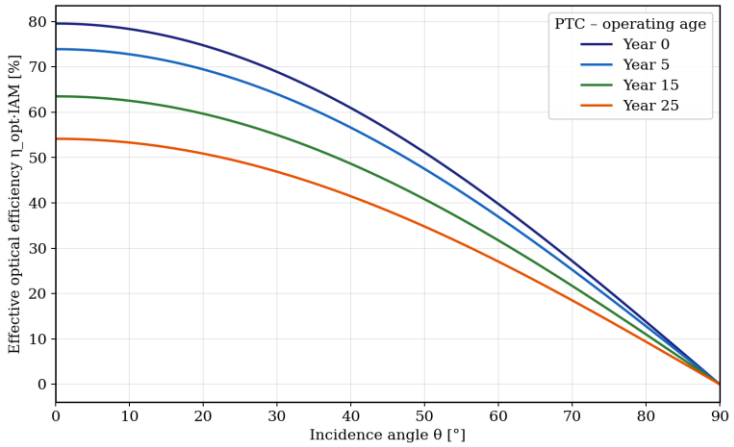

Figure 15. Effective optical efficiency of the PTC considering the Incidence Angle Modifier (IAM) for different service years. G_{normal}=800 W/m^2.

Figure 15 shows the effective optical efficiency η_{eff} (θ, t) =$\eta_{opt,\,PTC}(t)$. $IAM(\theta)$ as a function of the incidence angle (θ) (between the normal to the collector and the direct solar ray). The incidence angle factor (IAM or $K(\theta)$) models the loss associated with the angle: reduction in glass transmittance and stray reflections on the parabolic mirror. At (θ=0°) (normal incidence), (K=1) and efficiency are at its maximum; at (θ=60°, K≈0,72), representing a loss of approximately 28 % even for a new collector.

The combined effect of ageing and the angle of incidence is multiplicative and non-linear: for a PTC after 25 years at (θ=45°), the effective optical efficiency does not exceed (50%) of its initial optimal value. This highlights the crucial importance of the solar tracking system for

Power System Technology
ISSN:1000-3673

Received: 16-11-2025 Revised: 05-01-2026 Accepted: 23-03-2026

PTCs; an inaccuracy of (±2°) can lead to a (3–5%) loss in efficiency, amplified by degradation. These results corroborate the IAM models by Güven and Bannerot [19] as well as the experimental measurements by Almanza et al. [11].

4. CONCLUSION

This work presents a comprehensive numerical approach, based on the finite element method (FEM), to model and simulate the degradation of the thermal and optical performance of flat-plate (FPC) and parabolic trough (PTC) solar collectors over a 25-year lifespan. The main conclusions of this study are as follows:

a- Validity and robustness of the FEM formulation: discretisation of the energy balance equations using P1 (1D) and Q4 (2D) finite elements enabled the temperature fields to be solved accurately. Mesh convergence, verified by h-refinement analysis, confirms a relative error of less than 0.5%.

b- Precise quantification of degradation: over 25 years of operation, the PTC's thermal efficiency decreases by 22–28%, mainly due to a reduction in absorptance (-15%), a decrease in glazing transmittance (-18%) and an increase in the loss coefficient U_L (+55 %). The PTC suffers a degradation in optical efficiency of (14–18%), driven primarily by the deterioration of the parabolic mirror (-22% over rho_m).

c- Key role of fouling: the fouling resistance $Rf(t)$ reaches (75%) of its asymptotic value by the 7th year of operation, reducing the internal heat transfer coefficient $h_{i,eff}$ by26 %.

d- Universality of the degradation rate: the relative efficiency degradation rate converges towards approximately 1% per year for both types of collectors, under Mediterranean or semi-arid conditions.

e- Practical implications for Algeria: a preventive maintenance programme can reduce degradation by (40%), significantly improving the economic viability of solar thermal projects.

f- Future prospects: this model will be extended to incorporate transient thermal cycles, fracture mechanics models and thermomechanical coupling. Experimental validation on a solar test bench at the local university is also planned.

Bibliographical references

[1] Gouvernement Algérien — Agence Nationale pour la Promotion et la Rationalisation de l'Utilisation de l'Énergie (APRUE). Atlas solaire de l'Algérie. Éditions CDER, Alger, 2021.

Power System Technology
ISSN:1000-3673

Received: 16-11-2025 Revised: 05-01-2026 Accepted: 23-03-2026

[2] Bates J.M., Edwards R.D. — Performance degradation of flat plate solar collectors: a review. Solar Energy Materials and Solar Cells, 2019, vol. 198, pp. 37–48. DOI:10.1016/j.solmat.2019.03.022

[3] Biryukov S. — Determination of the thermal degradation rate of evacuated tube and flat-plate solar collectors. Solar Energy, 2016, vol. 125, pp. 235–241.

[4] Petter J., Elvestad H. — In situ testing of flat-plate solar collectors. Solar Energy, 2017, vol. 152, pp. 83–89.

[5] Chopra M., Sharma D., Singh O.P. — Finite element analysis of heat transfer in flat plate solar collectors. Energy Procedia, 2017, vol. 109, pp. 336–342.

[6] Al-Damook M., Khalil W.H. — Numerical investigation of solar flat plate collectors using a 2D finite element model. Thermal Science and Engineering Progress, 2020, vol. 18, 100528.

[7] Duffie J.A., Beckman W.A. — Solar Engineering of Thermal Processes. 4th ed. Wiley, New York, 2013. ISBN 978-0-470-87366-3.

[8] Kalogirou S.A. — Solar Energy Engineering: Processes and Systems. 2nd ed. Academic Press, Oxford, 2014. ISBN 978-0-12-397270-5.

[9] Saleh Im H., El Abbassi A., Azzouzi M. — Degradation kinetics of selective coatings on solar absorbers in desert climates. Applied Solar Energy, 2020, vol. 56, no. 3, pp. 181–190.

[10] Zondag H.A., de Boer R., Bakker M. — Long-term durability testing of solar thermal collectors under accelerated weathering. Energy and Buildings, 2019, vol. 205, p. 109525.

[11] Almanza R., Hernández P., Martinez I., Mazari M. — Development and mean life of aluminum first-surface mirrors for solar energy applications. Solar Energy Materials and Solar Cells, 2009, vol. 93, pp. 1647–1651.

[12] Benkert S., Widén J., Löfström E. — Long-term field monitoring of solar thermal flat-plate collectors in German residential buildings. Solar Energy, 2020, vol. 208, pp. 984–993.

[13] Brunold S., Frei U., Carlsson B. — Accelerated aging tests for solar energy materials: a study performed in the framework of the IEA Solar Heating and Cooling programme. Solar Energy Materials and Solar Cells, 2000, vol. 61, pp. 350–360.

[14] Garrett-Price B.A., et al. — Fouling of Heat Exchangers: Characteristics, Costs, Prevention, Control, and Removal. Noyes Publications, New Jersey, 1985.

Power System Technology
ISSN:1000-3673

Received: 16-11-2025 Revised: 05-01-2026 Accepted: 23-03-2026

[15] Heck N., Smith C., Farrell E. — LCCA of flat plate solar thermal systems in residential applications: a long-term analysis. Solar Energy, 2016, vol. 139, pp. 447–457.

[16] Flores V., Almanza R. — Behavior of the compound parabolic concentrator with a double-walled receiver. Solar Energy, 2004, vol. 76, pp. 173–179.

[17] Jordan D.C., Kurtz S.R. — Photovoltaic degradation rates — an analytical review. Progress in Photovoltaics: Research and Applications, 2013, vol. 21, pp. 12–29.

[18] IEA PVPS Task 13 — Technical Report T13-01. Performance and Reliability of Photovoltaic Systems. International Energy Agency, 2014.

[19] Güven H.M., Bannerot R.B. — Derivation of universal error limits for solar concentrators. Journal of Solar Energy Engineering, 1986, vol. 108, pp. 275–281.

[20] Hottel H.C., Whillier A. — Evaluation of flat-plate collector performance. Transactions of the Conference on the Use of Solar Energy, Vol. 2, Part I: Thermal Processes. University of Arizona Press, 1958, pp. 74–104.

Nomenclatures:	**Quantity**	**Unit**
Symbol		
$\alpha(t)$	Absorptance of the selective surface (degraded)	—
$\tau(t)$	Transmittance of the glazing (degraded)	—
$\rho_m(t)$	Reflectivity of the parabolic mirror (degraded)	—
$\varepsilon_a(t)$	Emittance of the PTC absorber tube (degraded)	—
η	Overall effective thermal efficiency	—
η_{opt}	Overall optical efficiency of the collector	—
F_R	Hottel-Whillier heat recovery factor	—
F'	Efficiency of the absorber plate fin	—
$U_L(t)$	Overall heat loss coefficient (gradient)	$W/m^2 \cdot K$
$R_f(t)$	Fouling resistance	$m^2 \cdot K/W$

Power System Technology
ISSN:1000-3673

Received: 16-11-2025 Revised: 05-01-2026 Accepted: 23-03-2026

h_i	Internal convection coefficient of the tube	W/m²·K
k_p	Thermal conductivity of the absorber plate	W/m·K
$\delta = t_f$	Thickness of the absorber plate	m
G	Direct normal irradiance (DNI)	W/m²
S(t)	Net solar flux absorbed by the panel	W/m²
T_{fi}	Inlet temperature of the heat transfer fluid	K
T_{amb}	Ambient temperature	K
T_{sky}	Effective sky temperature (radiation)	K
$\dot{m}_f$	Mass flow rate of the heat transfer fluid	kg/s
c_f	Specific heat of the heat transfer fluid	J/kg·K
C_r	Geometric concentration factor of the PTC	—
W_{ap}	Aperture width of the parabolic concentrator	m
K(θ)	Incidence angle modification factor (IAM)	—
Q_{rad}	Annular radiative losses (PTC tube)	W/m
Σ	Stefan-Boltzmann constant = 5.67×10^{-8}	W/m²·K⁴
K_e	Elemental stiffness matrix (MEF)	—
F_e	Elemental load vector (MEF)	—
N_i	Shape functions (finite elements)	—
H	Finite element size (mesh size)	m
E	Annual heat production	GJ/year
T	Collector service life	years